

When Sensing Varies with Contexts: Context-as-Transform for Tactile Few-Shot Class-Incremental Learning

Yifeng Lin¹, Aiping Huang¹, Wenxi Liu², Si Wu³, Tiesong Zhao^{†1}, Zheng-Jun Zha⁴

¹Fujian Key Laboratory for Intelligent Processing and Wireless Transmission of Media Information, College of Physics and Information Engineering, Fuzhou University, Fuzhou 350108, China ²College of Computer and Data Science, Fuzhou University, Fuzhou 350108, China ³School of Computer Science and Engineering, South China University of Technology, Fuzhou 350108, China ⁴MoE Key Laboratory of Brain-inspired Intelligent Perception and Cognition, University of Science and Technology of China, Hefei 230026, China

[†]Corresponding author.

Abstract: Few-Shot Class-Incremental Learning (FSCIL) can be particularly susceptible to acquisition contexts with only a few labeled samples. A typical scenario is tactile sensing, where the acquisition context (*e.g.*, diverse devices, contact state, and interaction settings) degrades performance due to a lack of standardization. In this paper, we propose Context-as-Transform FSCIL (CaT-FSCIL) to tackle the above problem. We decompose the acquisition context into a structured low-dimensional component and a high-dimensional residual component. The former can be easily affected by tactile interaction features, which are modeled as an approximately invertible Context-as-Transform family and handled via inverse-transform canonicalization optimized with a pseudo-context consistency loss. The latter mainly arises from platform and device differences, which can be mitigated with an Uncertainty-Conditioned Prototype Calibration (UCPC) that calibrates biased prototypes and decision boundaries based on context uncertainty. Comprehensive experiments on the standard benchmarks HapTex and LMT108 have demonstrated the superiority of the proposed CaT-FSCIL.

Project Page: The project page will be released.

MIC@FZU

1 Introduction

Real-world intelligent systems rarely operate under a static closed-set taxonomy. New classes continually emerge, while labels are often available for only a few examples. Few-Shot Class-Incremental Learning (FSCIL) captures this open-world requirement: a model is trained on base classes and then updated across multiple incremental sessions, each introducing novel classes from a few labeled examples, with evaluation over all classes observed so far. This setting combines the generalization challenge of few-shot learning with the stability challenge of continuous learning under evolving distributions.

Nowadays, FSCIL has a widespread application from vision to EEG [13], audio [17], and other modalities [14, 31]. However, cross-domain FSCIL exposes a common bottleneck: many methods assume that intra-class variations can be implicitly absorbed by the embedding, yet when sensing depends strongly on acquisition contexts (*e.g.*, diverse devices, contact states, and interaction settings), few-shot prototypes and decision boundaries formed during incremental sessions can be systematically distorted. This issue is particularly severe in tactile sensing. As shown in fig. 1, the primary challenge of tactile FSCIL is not merely having fewer labeled samples, but the strong context effects in tactile representations. As

a result, the variation of the same material across contexts can exceed the difference between different materials under similar contexts. Consequently, FSCIL models tend to exploit context shortcuts and may even overfit to context-dependent cues, resulting in unstable material representations and brittle generalization across contexts.

In this paper, we make the first attempt to address tactile sensing with an variation of FSCIL. We represent the structured and repeatable part of acquisition context as a low-dimensional component, and treat the remaining complex and hard-to-estimate factors as a highly abstract high-dimensional residual component. Based on this decomposition, we propose CaT-FSCIL, a Context-as-Transform framework that explicitly canonicalizes context-dependent observations: we model the low-dimensional context as an approximately invertible transform family and optimize it using a pseudo-context consistency loss, and we further introduce Uncertainty-Conditioned Prototype Calibration (UCPC) to compensate for residual context effects and mitigate prototype bias and boundary miscalibration under context variations. In summary, our contributions are as follows:

- We propose CaT-FSCIL, a Context-as-Transform framework that explicitly canonicalizes context-dependent observations by learning an approximately invertible low-dimensional context transform, which mitigates proto-

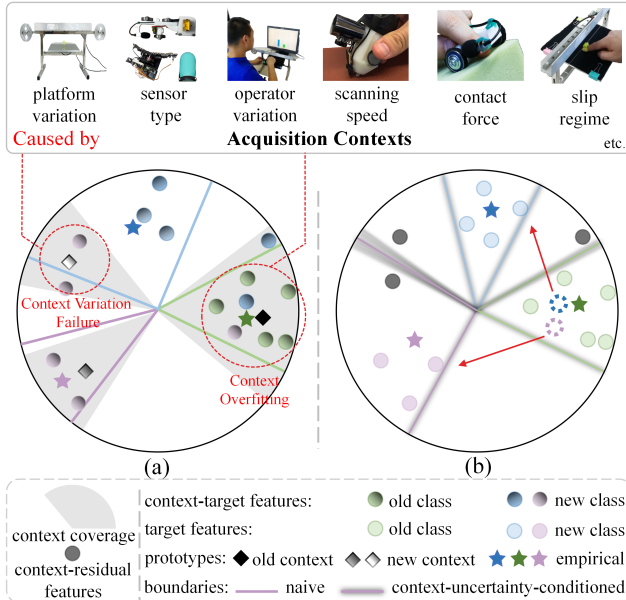


Figure 1 Acquisition context degrades FSCIL through two coupled failure modes. (a) Context overfitting makes prototypes encode context-dependent cues and yields unstable target representations. Context variation failure occurs when a novel acquisition context is interpreted as the closest previously observed one. (b) CaT-FSCIL applies a learned context transform to canonicalize the context-target feature into a more compact target representation, while handling the residual via context uncertainty to calibrate decision boundaries and mitigate misclassification.

type bias under diverse acquisition contexts of tactile sensing.

- We introduce a pseudo-context consistency loss that trains the context estimator using pseudo-contexts sampled from a bounded uniform distribution, improving robustness under unobserved contexts.
- We develop UCPC, which leverages context uncertainty to condition prototype shrinkage and boundary sharpness, mitigating overconfident predictions and misattribution under residual high-dimensional context variations.

2 Related Work

Few-shot class-incremental learning was initially introduced in TOPIC [29] and has since increasingly adopted a paradigm that decouples feature representation learning from classifier updates [36, 38]. Recent studies have moved toward richer model structures and stronger transfer from large-scale pretraining, and can be broadly categorized into boundary-based [23, 8, 15], prompt-based [22, 20], and replay-based [1, 2, 11] approaches. Beyond these lines, Comp-FSCIL [39] explores compositional reasoning by de-

composing class knowledge and recombining it for inference, while methods such as Lark [25] and Flexi-FSCIL [32] focus on continual adaptation via lightweight parameter editing or efficient model fusion. However, as noted above, the majority of FSCIL algorithms are validated primarily on image benchmarks [12, 30, 24]. To address practical needs, FSCIL has been extended to domains such as physiological signals [21, 27, 13], graphs [28], and audio [16, 17]. In multi-modal settings, VT-CIL [7] studies class-incremental learning jointly over vision and touch through a unified model with cross-modal regularization. TIFS [31] instead leverages tactile cues to synthesize imagined visual observations, using the generated visuals as auxiliary guidance to improve alignment and forgetting resistance. Despite these advances, FSCIL that explicitly accounts for acquisition-context effects, particularly in purely tactile sensing, remains largely underexplored.

Tactile datasets can be broadly categorized into two types: visual-tactile [18, 34, 6] and numerical-tactile [26, 10, 35]. The former uses optical tactile sensors to record contact-induced deformations as images, which facilitates geometric representation learning and alignment with visual features for cross-modal learning. Such visual-tactile sensors typically incorporate compliant, deformable media (*e.g.*, silicone elastomers), and they tend to be more expensive. In contrast, numerical-tactile datasets are collected using inertial, force, torque, or related sensors that capture one-dimensional or low-dimensional time-series signals. Most such sensors are built with rigid materials, making them cheaper and more durable. However, they often rely on scanning platforms that require high-precision control. The raw data in the HapTex [10] and LMT108 [26] datasets used in this work are numerical-tactile in nature and comply with the IEEE 1918.1.1 standard [9].

Tactile-based object recognition with numerical tactile signals has progressed with slip sensing for texture recognition [3] and hybrid triboelectric-capacitive designs that disentangle surface texture from hardness for deep learning-assisted object recognition [33]. At the model level, convolutional networks learn from voltage waveforms of tactile arrays [19], recurrent models aggregate contacts from soft grippers for object recognition [5], and triboelectric multi-modal sensing supports joint inference of material, curvature, and pressure [37]. Beyond closed-set learning, zero-shot tactile texture recognition leverages visual and semantic priors [4].

3 Methodology

3.1 Problem Definition

Few-Shot Class-Incremental Learning proceeds through sessions $\{\ell_0, \ell_1, \dots, \ell_S\}$, where ℓ_0 denotes the base session and ℓ_i ($0 < i \leq S$) denotes the i -th incremental session. Session ℓ introduces a disjoint label set \mathcal{Y}_ℓ , with $\mathcal{Y}_\ell \cap \mathcal{Y}_{\ell'} = \emptyset$ for $\ell \neq \ell'$. In session ℓ , the learner has access only to $\mathcal{D}_\ell = \{(x_{i,\ell}, y_{i,\ell})\}_{i=1}^{n_\ell}$, where n_ℓ is the number of labeled

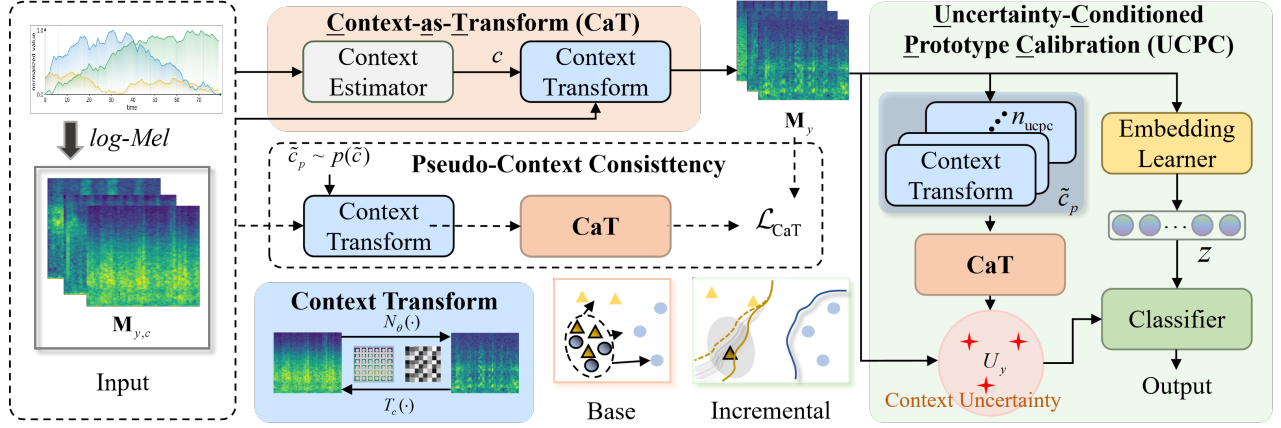


Figure 2 The context transform is the core operation of Context-as-Transform (CaT), which uses low-dimensional context parameters to modulate acquisition-context effects and is shared across all modules in CaT-FSCIL. (i) At inference, the estimated context c is used to canonicalize the observed spectrogram $M_{y,c}$ into a material-centric representation M_y , which is fed to the embedding learner and UCPC. (ii) During training, pseudo-contexts \tilde{c}_p are injected to optimize the context estimator via pseudo-context consistency. (iii) In UCPC, n_{ucpc} pseudo-contexts are sampled to estimate context uncertainty from canonicalization stability and calibrate the classifier.

samples, $x_{i,\ell}$ is a tactile observation, and $y_{i,\ell} \in \mathcal{Y}_\ell$ is its label. For $\ell \geq 1$, each incremental session follows an N -way K -shot protocol: $|\mathcal{Y}_\ell| = N$, and each novel class $y \in \mathcal{Y}_\ell$ provides a support set $S_y = \{(x_{i,\ell}, y_{i,\ell}) \in \mathcal{D}_\ell : y_{i,\ell} = y\}$ with $|S_y| = K$. After updating on session ℓ , evaluation is performed over $\mathcal{Y}_{\leq \ell} = \bigcup_{j=0}^{\ell} \mathcal{Y}_j$ to assess both novel-class acquisition and retention.

Acquisition context. We define acquisition context as systematic, repeatable shifts induced by the sensing pipeline, consisting of (i) a structured low-dimensional component amenable to explicit parameterization and (ii) a high-dimensional residual. We therefore model low-dimensional context via Context-as-Transform and introduce UCPC to mitigate the effect of the unmodeled residual component.

3.2 Overall Framework

We propose CaT-FSCIL, a framework for Few-Shot Class-Incremental Learning under context effects, as illustrated in fig. 2. The core component is Context-as-Transform (CaT). Given an input tactile sample x , represented as a short temporal segment of time-series signals, we first convert it into a multi-channel log-Mel spectrogram:

$$\mathbf{M} = \text{Mel}(x). \quad (1)$$

The log-Mel spectrogram parameter settings are provided in the Appendix section A. For the same material, different structured low-dimensional component of acquisition context (e.g., scanning speed, contact force, coupling, and micro-slip states), can produce markedly different log-Mel spectrograms. We summarize the context effect via a transformation family and a residual mismatch term:

$$\mathbf{M}_{y,c} = T_c(\mathbf{M}_y) + \epsilon. \quad (2)$$

Importantly, this additive form is an approximation in the log-Mel representation, rather than an assumption that the underlying physical effects are additive. Here, $M_{y,c}$ is the observed spectrogram for material class y under context c , M_y is the material-canonical spectrogram, and $T_c(\cdot)$ denotes the context transform family. The residual ϵ captures the discrepancy between the true acquisition process and our transform model, aggregating few-shot noise, limited context coverage, and high-dimensional residual effects not captured by the low-dimensional parameterization of T_c .

We do not explicitly parameterize these high-dimensional residual effects, since doing so is difficult to identify from few-shot supervision and can introduce costly, tightly coupled modeling that interferes with learning material-discriminative embeddings. For notational simplicity, we omit ϵ in the following derivation, while the proposed objectives are designed to mitigate its impact.

Given an observed spectrogram $M_{y,c}$, we first estimate its acquisition context using a context estimator g_θ , which predicts the low-dimensional context parameters c . We then instantiate a canonicalization operator $N_\theta(\cdot)$ based on c and apply an approximate inverse context transform, producing a canonicalized spectrogram M_y that better reflects the underlying material-intrinsic signal. We then encode M_y using an embedding learner f_θ implemented as a standard ResNet-18 backbone, yielding an embedding z . Finally, a classifier h_θ predicts labels over the current class set.

Concretely, h_θ samples a stochastic prototype $\tilde{\mu}_y$ from $\mathcal{N}(\mu^{\text{ucpc}}, \sigma^{\text{ucpc}})$ and performs cosine-similarity prediction:

$$\tilde{y} = \arg \max_y \frac{e^{\cos(z, \tilde{\mu}_y)}}{\sum_{h \in \mathcal{Y}_{\leq \ell}} e^{\cos(z, \tilde{\mu}_h)}}. \quad (3)$$

The classifier is learnable rather than fixed across sessions. In particular, μ^{ucpc} and σ^{ucpc} are trainable, and UCPC maintains

per-class centers and scales $\{\mu_y^{\text{ucpc}}, \sigma_y^{\text{ucpc}}\}$. By calibrating prototypes and decision-boundary parameters according to context uncertainty, UCPC mitigates prototype bias and excessive boundary rigidity, which reduces overconfident novel-class predictions and misattribution to previously learned classes during incremental learning. In this way, UCPC reduces the classifier’s sensitivity to residual context variability beyond the explicit low-dimensional context model, especially in later incremental sessions.

3.3 Context-as-Transform Canonicalization

Context Transform Family. We model acquisition-context effects as a family of approximately invertible transformations $T_c(\cdot)$ acting on the log-Mel spectrogram. The low-dimensional context variable c summarizes factors such as scanning speed, applied pressure, and contact state. These factors induce structured, low-dimensional distortions in the log-Mel representation, including (i) a frequency-axis translation δ , (ii) a temporal scaling τ of frictional texture patterns, (iii) a global energy bias b that correlates with force–speed interactions, and (iv) a tilt s of the spectral envelope. We therefore parameterize the low-dimensional context transform as the composition of a differentiable geometric warp and an amplitude modulation:

$$T_c(\mathbf{M}_y) = \mathcal{A}_{b,s}(\mathcal{G}_{\delta,\tau}(\mathbf{M}_y)), c = (\delta, \tau, b, s). \quad (4)$$

Geometric warp. We treat M_y as a 2D feature map and apply the same geometric transform independently to each channel. Let $\text{Grid}(\cdot)$ denote the standard bilinear sampling operator. Using a sampling grid $\Pi_{\delta,\tau}$ constructed by composing translation and scaling, the warp is written as

$$\begin{aligned} \mathcal{G}_{\delta,\tau}(\mathbf{M}_y) &= \text{Grid}(\mathbf{M}_y, \Pi_{\delta,\tau}), \\ \Pi_{\delta,\tau}(v) &= \text{clip}\left(\frac{v - \Delta_v}{\kappa_v}, -1, 1\right), \end{aligned} \quad (5)$$

where v indexes either the frequency or time axis, Δ_v denotes the axis-wise translation, and κ_v denotes the axis-wise scaling. Here, $\text{clip}(\cdot, -1, 1)$ constrains the normalized coordinates to $[-1, 1]$ to avoid out-of-range sampling.

Amplitude modulation. We approximate low-dimensional context-dependent energy variation with an additive envelope,

$$\mathcal{A}_{b,s}(\mathbf{M}_y) = \mathbf{M}_y + b + s \cdot r_f, \quad (6)$$

where r_f is a normalized frequency coordinate. This coordinate yields a differentiable and interpretable parameterization of spectral-envelope changes using two scalars (b, s) . Concretely, for a log-Mel spectrogram with F Mel bins, let $f \in \{0, 1, \dots, F - 1\}$ be the frequency index and define

$$r_f = \frac{2f}{F - 1} - 1 \in [-1, 1]. \quad (7)$$

Finally, when c lies within a reasonable range, the resulting transform $T_c(\cdot)$ is approximately invertible under discrete

sampling. This property motivates the context estimator used for inverse-transform canonicalization.

Context estimator and canonicalization. CaT learns a low-dimensional context estimator g_θ that predicts $c = (\delta, \tau, b, s)$ from an input spectrogram. We instantiate g_θ as a lightweight convolutional network with three residual convolutional blocks, followed by global average pooling and a linear head, which simplifies optimization while retaining sufficient capacity. To keep the predicted parameters numerically stable and to maintain approximate invertibility, we bound the raw outputs of g_θ using squashing functions: δ is mapped by $\tanh(\cdot)$ and τ by $\text{sigmoid}(\cdot)$. The resulting canonicalization operator $N_\theta(\cdot)$ applies an estimated inverse transform,

$$\begin{aligned} N_\theta(\mathbf{M}_{y,c}) &= T_c^{-1}(\mathbf{M}_{y,c}), \\ T_c^{-1}(\mathbf{M}_{y,c}) &\triangleq \mathcal{G}_{-\delta, 1/\tau}(\mathbf{M}_{y,c} - b - s \cdot r_f), \\ c = (\delta, \tau, b, s) &= g_\theta(\mathbf{M}_{y,c}). \end{aligned} \quad (8)$$

This explicit canonicalization removes low-dimensional context-induced variation through an estimated inverse transform, rather than delegating context–material disentanglement entirely to deep features. The distinction is especially important in FSCIL under context effects, where novel classes are observed under only a few contexts, making purely implicit learning prone to prototype bias and poor cross-context generalization in the incremental sessions.

3.4 Pseudo-Context Consistency

An optimal context estimator should recover accurate context parameters. Equivalently, for the same material instance, canonicalizing an observation after an arbitrary context perturbation should match the canonicalization of the unperturbed sample. In practice, however, true contexts are often unobservable or only partially specified. We therefore introduce pseudo-contexts \tilde{c}_p to cover unknown residual factors and enforce canonicalization stability under this perturbation family. Specifically, we sample pseudo-contexts from a bounded uniform distribution $p(c)$ and apply the corresponding context transform to the log-Mel spectrogram:

$$\mathbf{M}_{y,c,\tilde{c}_p} = T_{\tilde{c}_p}(\mathbf{M}_{y,c}), \tilde{c}_p \sim p(c), \quad (9)$$

thereby defining the pseudo-context consistency loss as:

$$\mathcal{L}_{\text{CaT}} = \mathbb{E}_{\tilde{c}_p \sim p(c)} [\|N_\theta(\mathbf{M}_{y,c,\tilde{c}_p}) - N_\theta(\mathbf{M}_{y,c})\|_1]. \quad (10)$$

During optimization, gradients are propagated only through the pseudo-context branch $N_\theta(\mathbf{M}_{y,c,\tilde{c}_p})$, while the anchor branch $N_\theta(\mathbf{M}_{y,c})$ is treated as a stop-gradient target to anchor the reference. The use of ℓ_1 norm is justified in Appendix section C. This design prevents the anchor representation from drifting, avoiding collapse, and forces the estimator to learn parameters that invert context-induced effects. As a result, the canonicalized representation becomes more robust to unobserved residual contexts, which improves transferability in incremental sessions.

3.5 Uncertainty-Conditioned Prototype Calibration

CaT explicitly canonicalizes low-dimensional context-dependent observations via an inverse transform, yet prototype bias can still emerge during incremental updates. With only a few shots and limited context coverage for novel classes, the prototype estimate $\hat{\mu}_y$ can be systematically displaced from the material-centric representation. UCPC addresses this issue by using canonicalization stability as a proxy for context uncertainty. It then performs uncertainty-aware prototype μ shrinkage in an empirical Bayes manner and calibrates the decision-boundary scale σ to mitigate miscalibration in incremental sessions, particularly when residual high-dimensional acquisition-context factors remain unmodeled.

Context uncertainty as instability under pseudo-contexts. CaT is expected to remove context-induced variation, so canonicalization should be stable under additional pseudo-context perturbations of the same sample. Large deviations from this stability suggest that the sample is influenced by context factors that differ from those encountered in previously learned classes, and thus indicate higher uncertainty.

We estimate sample-wise uncertainty by sampling n_{ucpc} pseudo-contexts and measuring the dispersion of canonicalized representations. For each pseudo-context instance indexed by i , we apply a pseudo-context transform to obtain a perturbed feature map $\mathbf{M}_{y,\tilde{c}_p}^{(i)}$ and compute its deviation from the canonicalization of the unperturbed observation:

$$u(x) = \frac{1}{n_{\text{ucpc}}} \sum_{i=1}^{n_{\text{ucpc}}} \left\| N_{\theta}(\mathbf{M}_{y,\tilde{c}_p}^{(i)}) - N_{\theta}(\mathbf{M}_{y,c}) \right\|_1, \quad (11)$$

$$\mathbf{M}_{y,\tilde{c}_p}^{(i)} = T_{\tilde{c}_p}^{(i)}(\mathbf{M}_y).$$

The use of ℓ_1 norm is justified in Appendix section C. If a sample is poorly explained by the context estimator, its underlying context may deviate from the assumed context range (e.g., the pseudo-context distribution) or even fall outside it, leading to high sample-wise uncertainty. For a class y with support set S_y , we aggregate this signal and define the class-level context uncertainty as

$$U_y = \frac{1}{|S_y|} \sum_{x \in S_y} u(x), \quad (12)$$

where U_y provides a computable, actionable measure of residual context uncertainty at the class level, indicating whether the context coverage is sufficiently manageable for effective uncertainty calibration, by evaluating canonicalization stability under the specified perturbation family.

Shrinkage as a posterior mean with uncertainty-dependent effective sample size. For a novel class y , we model its true material center μ_y^* with a Gaussian prior that summarizes previously learned classes, and treat the support-set prototype μ_y as a noisy observation:

$$\mu_y^* \sim \mathcal{N}(\mu_p, \Sigma_p), \quad \mu_y | \mu_y^* \sim \mathcal{N}(\mu_y^*, \Sigma_y). \quad (13)$$

Here, Σ_p encodes the prior dispersion of class centers in the embedding space, while Σ_y captures the uncertainty of the few-shot prototype. Assuming isotropic covariance, we use $\Sigma_p = \sigma_p^2 I$ and $\Sigma_y = \sigma_y^2 I$. The prior statistics (μ_p, σ_p^2) are computed from the embedding space based on previously learned classes, yielding a global reference for shrinkage.

In FSCIL under context effects, the prototype uncertainty Σ_y is dominated by few-shot noise and insufficient context coverage. We connect this term to the class-level context uncertainty by setting σ_y^2 to be a monotone increasing function of U_y . With these assumptions, the posterior is Gaussian and yields the precision-weighted posterior mean and variance:

$$\mathbb{E}[\mu_y^* | \mu_y] = \left(\frac{\sigma_p^{-2}}{\sigma_p^{-2} + \sigma_y^{-2}} \right) \mu_p + \left(\frac{\sigma_y^{-2}}{\sigma_p^{-2} + \sigma_y^{-2}} \right) \mu_y,$$

$$\mathbb{D}[\mu_y^* | \mu_y] = (\sigma_p^{-2} + \sigma_y^{-2})^{-1}, \quad (14)$$

which can be rewritten as:

$$\mu_y^{\text{ucpc}} = (1 - \lambda_y) \mu_y + \lambda_y \mu_p,$$

$$\sigma_y^{\text{ucpc}} = (\sigma_p^{-2} + \sigma_y^{-2})^{-1}. \quad (15)$$

This form makes the effect of uncertainty explicit. As U_y increases, σ_y^2 increases, which reduces the effective precision of the few-shot prototype and increases λ_y , leading to stronger shrinkage toward the prior mean μ_p . At the same time, the posterior variance increases, so sampling in h_{θ} becomes more dispersed and the induced decision boundary becomes less sharp, mitigating overconfident predictions under context bias. When U_y is small, the posterior concentrates and the classifier can rely more on the class-specific prototype without undue shrinkage or smoothing.

3.6 Final Loss Function

We optimize different objectives in the base and incremental sessions of FSCIL. Following PITS-SC [17], the base session includes pretraining and full training. We jointly train the representation and CaT canonicalization modules using a classification loss and the CaT-specific consistency objective. In incremental sessions, we supervise new classes and regularize the classifier with stored class-mean embeddings of past classes to mitigate forgetting. Concretely, we use the following losses:

$$\mathcal{L}_{\text{Base}} = \mathcal{L}_{\text{CE}} + \lambda_1 \mathcal{L}_{\text{CaT}} + \lambda_2 \mathcal{L}_{\text{Reg}}, \quad (16)$$

$$\mathcal{L}_{\text{Inc}} = \mathcal{L}_{\text{New}} + \lambda_3 \mathcal{L}_{\text{Old}},$$

where $\lambda_1, \lambda_2, \lambda_3$ are weights, and \mathcal{L}_{CE} is the standard cross-entropy classification loss. The terms are defined as

$$\mathcal{L}_{\text{New}} = -\log \left(\frac{e^{\cos(z, \tilde{\mu}_y^{\text{ucpc}})}}{\sum_{h \in \mathcal{Y}_{\ell}} e^{\cos(z, \tilde{\mu}_h^{\text{ucpc}})}} \right),$$

$$\mathcal{L}_{\text{Old}} = -\log \left(\frac{e^{\cos(\mu, \tilde{\mu}_y^{\text{ucpc}})}}{\sum_{h \in \mathcal{Y}_{\leq \ell}} e^{\cos(\mu, \tilde{\mu}_h^{\text{ucpc}})}} \right). \quad (17)$$

Here, \mathcal{L}_{Reg} penalizes excessively large context parameters to avoid degenerate context transforms. In \mathcal{L}_{Old} , μ denotes the stored class-mean embedding of an old class indexed by y' , and the summation index h ranges over class labels.

4 Experiment

4.1 Datasets

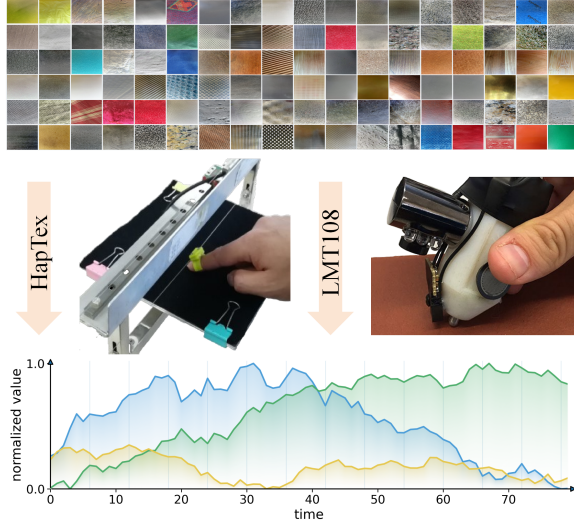


Figure 3 Photographs show example materials from LMT108. HapTex groups materials into coarse categories (*e.g.*, velvet, leather, chiffon, wool, nylon, polyester, linen, and silk). LMT108 defines nine coarse categories, including meshes, stones, blank glossy surfaces, wood types, rubbers, fibers, foams, foils and papers, and textiles and fabrics. We apply dataset-specific normalization for numerical stability and ease of use. Context-dependent variations persist after this preprocessing, motivating CaT-FSCIL.

We construct two datasets to evaluate tactile FSCIL from the raw HapTex [10] and LMT108 [26] data. Both are representative numerical–tactile benchmarks and are aligned with the IEEE 1918.1.1 standard format [9] in practice. The acquisition setups are shown in fig. 3.

HapTex is collected with a TexRecorder system that combines a force sensor (normal and friction forces) and a high-resolution grating displacement sensor (sliding displacement). It contains 120 material classes with time-series measurements of friction force, normal force, friction coefficient, displacement, and velocity. In addition, HapTex provides scanned texture images for each material, which enables appearance-based modeling in some cases.

LMT108 is collected using a handheld Texplorer that supports multimodal tactile sensing. The probe uses a hemispherical stainless-steel tip and integrates a triaxial accelerometer, microphone, infrared reflectance sensor, camera, and dual force-sensitive resistors. Tactile-related signals are captured

by an NI DAQ at 10 kHz. The dataset covers 108 material classes and provides synchronized multimodal observations, including acceleration, friction, reflectance, audio, metal detection, and images at high resolution.

Table 1 Preprocessed Dataset Details

Dataset	Sampling Rate (Hz)	Sample Length (s)	Category (Coarse/Fine)	Num./Category
Haptex	1K	0.5	10/120	100
LMT108	10K	0.8	9/108	120

We slice the raw sequences into short segments and summarize the configurations in table 1. To reflect short contacts in practical scenarios, we use slice lengths of 0.5 s (HapTex) and 0.8 s (LMT108). Each segment is annotated with both coarse and fine-grained labels. Unless otherwise stated, we use only the fine-grained labels in this work throughout.

4.2 Implementation Details

Baselines and evaluation protocol. We compare CaT-FSCIL against PriViLege [22], Comp-FSCIL [39], OrCo [2], ADBS [15], and PITS-SC [17], using official code for all methods. Since most baselines were developed for image benchmarks (except PITS-SC for audio), we standardize inputs by uniformly converting tactile signals to log–Mel spectrograms and evaluate under a standard 5-way 5-shot protocol. We report averages over five runs with the same fixed random seeds for all methods.

Optimization. We train all models with SGD. We use learning rates of 0.1 (pretraining), 0.01 (full base), and 0.1 (incremental), for 100, 10, and 200 epochs, respectively, with the learning rate decayed by a factor of 0.5 every 40 epochs. We set λ_1 , λ_2 , and λ_3 to 0.05, 10^{-4} , and 1.0, respectively. For UCPC, we use n_{ucpc} of 20 on HapTex and 30 on LMT108. These settings are kept fixed across runs and methods to ensure comparability. Experiments are implemented in PyTorch on a single NVIDIA A40 GPU.

Metrics. We evaluate all methods using Average Accuracy (AA), Performance Drop (PD), and Average Drop Rate (ADR). Let Acc_ℓ denote the accuracy after session ℓ , evaluated on the cumulative label space containing all classes observed up to ℓ . Intuitively, AA measures overall performance averaged across sessions, PD reflects end-to-end degradation from base to final, and ADR captures the average relative drop between successive sessions:

$$\text{AA} = \frac{1}{S+1} \sum_{\ell=0}^S \text{Acc}_\ell, \quad (18)$$

$$\text{PD} = \text{Acc}_0 - \text{Acc}_S, \quad (19)$$

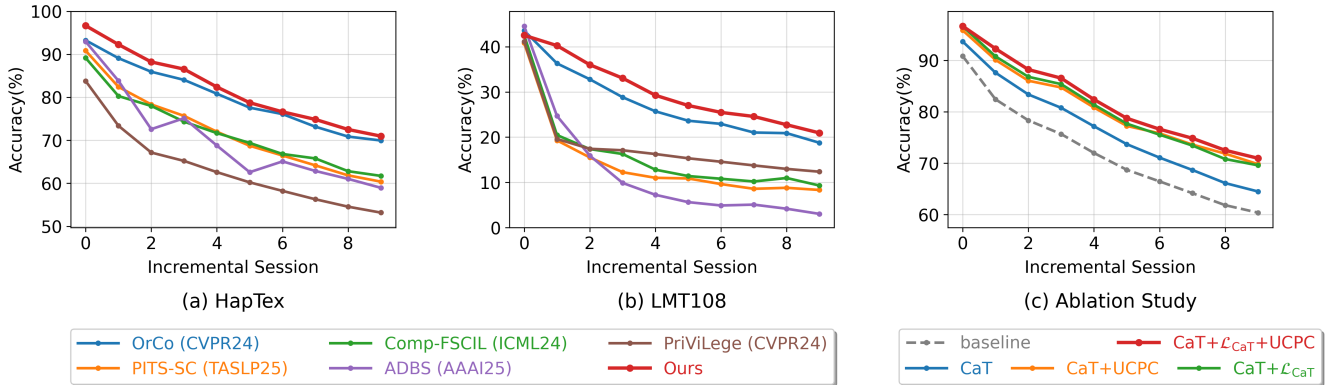
$$\text{ADR} = \frac{1}{S} \sum_{\ell=0}^{S-1} \frac{\text{Acc}_\ell - \text{Acc}_{\ell+1}}{\text{Acc}_\ell}. \quad (20)$$

Table 2 Comparison on the HapTex dataset. Red and blue denote the best and second-best results, respectively.

Method	Accuracy in each session (%) \uparrow										PD \downarrow	AA \uparrow	ADR \downarrow
	0	1	2	3	4	5	6	7	8	9			
PriViLege[22]	83.79	73.38	67.15	65.20	62.59	60.22	58.23	56.29	54.56	53.18	30.61	63.46	4.38
ADBS[15]	92.95	83.83	72.58	75.13	68.77	62.58	65.09	62.87	61.02	58.95	34.00	70.38	4.29
Comp-FSCIL[39]	89.15	80.28	77.98	74.33	71.67	69.38	66.81	65.78	62.81	61.72	27.43	71.99	3.58
PITS-SC[17]	90.83	82.42	78.33	75.67	71.99	68.72	66.46	64.17	61.84	60.38	30.45	72.08	3.97
OrCo[2]	93.25	89.09	85.93	84.04	80.82	77.58	76.09	73.16	70.86	69.95	23.30	80.08	2.82
CaT-FSCIL	96.65	92.27	88.21	86.54	82.39	78.74	76.61	74.85	72.51	70.96	25.69	81.97	3.03

Table 3 Comparison on the LMT108 dataset.

Method	Accuracy in each session (%) \uparrow										PD \downarrow	AA \uparrow	ADR \downarrow
	0	1	2	3	4	5	6	7	8	9			
ADBS[15]	44.54	24.70	15.92	9.88	7.25	5.63	4.89	5.08	4.17	3.03	41.51	12.51	22.15
PITS-SC[17]	40.84	19.29	15.52	12.26	11.01	10.87	9.62	8.58	8.80	8.32	32.52	14.51	13.00
Comp-FSCIL[39]	42.54	20.47	17.37	16.28	12.81	11.40	10.80	10.20	10.97	9.30	33.24	16.21	12.41
PriViLege[22]	41.17	19.61	17.43	17.10	16.27	15.33	14.57	13.75	12.98	12.36	28.81	18.06	9.70
OrCo[2]	43.57	36.32	32.81	28.84	25.72	23.64	22.94	21.03	20.89	18.76	24.81	27.45	7.95
CaT-FSCIL	42.54	40.26	36.02	33.06	29.27	27.01	25.48	24.58	22.75	20.94	21.60	30.19	6.79

**Figure 4** Performance comparison and ablation results. (a) HapTex, (b) LMT108, and (c) ablation on HapTex. CaT-FSCIL achieves the strongest overall performance across both datasets and remains robust to tactile-specific context-material entanglement, which can otherwise distort representations and impair FSCIL baselines.

We use AA as the primary metric since it summarizes overall performance across sessions in a single scalar, while PD and ADR complement it by quantifying performance degradation and stability over incremental updates.

4.3 Experimental Results

Results on HapTex and LMT108 are summarized in table 2, table 3, and fig. 4 (a) (b). Our method attains the best AA on both datasets and achieves lower PD and ADR.

The comparisons also highlight practical limitations of representative paradigms under context effects. Prompt-based FSCIL is constrained in tactile sensing because tactile founda-

tion models and large-scale tactile-text pairs are still limited in the current literature. Replay-based methods can improve context coverage by storing and replaying real samples, but this benefit comes with a storage-accuracy trade-off that must be evaluated under an explicit memory budget. Boundary-based methods can be sensitive to context bias, since calibrating decision boundaries without mitigating context dependence may amplify spurious context cues.

Notably, CaT-FSCIL outperforms the replay-based reference that uses real-sample replay, and it exceeds other methods evaluated under the same no-replay protocol, while storing only class-mean vectors for past classes.

Table 4 Ablation study on HapTex dataset.

CaT	\mathcal{L}_{CaT}	UCPC	Accuracy in each session (%) \uparrow										PD \downarrow	AA \uparrow	ADR \downarrow
			0	1	2	3	4	5	6	7	8	9			
×	×	×	90.83	82.42	78.33	75.67	71.99	68.72	66.46	64.17	61.84	60.38	30.45	72.08	3.97
✓	×	×	93.66	87.60	83.37	80.77	77.18	73.70	71.08	68.68	66.13	64.50	29.16	76.67	3.65
✓	×	✓	95.83	90.09	86.04	84.73	80.83	77.25	75.81	73.62	71.86	69.81	26.02	80.59	3.10
✓	✓	×	96.60	90.77	86.80	85.38	81.38	77.69	75.54	73.43	70.81	69.59	27.01	80.80	3.21
✓	✓	✓	96.65	92.27	88.21	86.54	82.39	78.74	76.61	74.85	72.51	70.96	25.69	81.97	3.03

4.4 Ablation Study

We conduct ablation studies on HapTex to assess the contributions of CaT-FSCIL (ablations on LMT108 are provided in the Appendix section B). Results are summarized in table 4 and fig. 4(c). We make three main observations.

First, CaT consistently improves performance, indicating that low-dimensional context canonicalization alleviates context-material entanglement and strengthens material discrimination in the base session while improving retention and novel-class performance in incremental sessions. Second, pseudo-context consistency provides a stronger training signal for the context estimator. In addition to \mathcal{L}_{CE} , optimizing \mathcal{L}_{CaT} encourages stable canonicalization under context perturbations, improving performance in our setting. Third, UCPC remains effective across settings. Even when the context estimator is trained without \mathcal{L}_{CaT} , UCPC yields gains by calibrating prototypes and softening overly rigid boundaries through uncertainty-conditioned shrinkage. When \mathcal{L}_{CaT} is enabled, class-wise uncertainty is reduced, so the marginal gain from UCPC becomes smaller but non-negligible. Overall, each component contributes to the final results.

We study how the pseudo-context sampling count n_{ucpc} used to estimate UCPC uncertainty affects overall performance (fig. 5). On HapTex, CaT-FSCIL becomes stable once n_{ucpc} is sufficiently large, exhibiting only minor fluctuations across sampling counts in repeated trials. This trend matches the intuition that small n_{ucpc} produces a high-variance uncertainty estimate and can therefore destabilize calibration. In contrast, performance on LMT108 shows a more pronounced dependence on n_{ucpc} . One plausible explanation is that LMT108 exhibits a richer and more heterogeneous context structure, where high-dimensional residual context factors may play a larger role. In this case, the bounded pseudo-context distribution provides an imperfect approximation to the true variability, making the method more sensitive to the particular sampling realization.

5 Conclusion

This paper addresses FSCIL under acquisition context variations, which is a prevalent yet challenging problem in emerging modalities such as tactile sensing. We propose CaT-

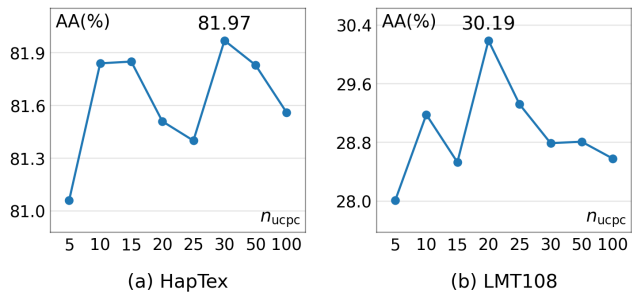


Figure 5 Effect of the pseudo-context sampling count n_{ucpc} on performance for (a) HapTex and (b) LMT108. HapTex is comparatively stable across n_{ucpc} , LMT108 shows larger variation.

FSCIL, a novel framework that robustifies FSCIL through an approximately invertible Context-as-Transform module and an UCPC module. Our design enables robust representation and classifier learning despite limited context coverage. Extensive experiments on benchmark datasets demonstrate consistent improvements over baselines and underscore CaT-FSCIL’s potential for application in new sensory modalities.

References

- [1] Aishwarya Agarwal, Biplab Banerjee, Fabio Cuzzolin, and Subhasis Chaudhuri. Semantics-driven generative replay for few-shot class incremental learning. In *Proceedings of the 30th ACM International Conference on Multimedia*, pages 5246–5254, 2022. 2
- [2] Noor Ahmed, Anna Kukleva, and Bernt Schiele. Orco: Towards better generalization via orthogonality and contrast for few-shot class-incremental learning. In *Proceedings of the IEEE/CVF Conference on Computer Vision and Pattern Recognition*, pages 28762–28771, 2024. 2, 6, 7
- [3] Ningning Bai, Yiheng Xue, Shuiqing Chen, Lin Shi, Junli Shi, Yuan Zhang, Xingyu Hou, Yu Cheng, Kaixi Huang, Weidong Wang, et al. A robotic sensory system with high spatiotemporal resolution for texture recognition. *Nature Communications*, 14(1):7121, 2023. 2
- [4] Guanqun Cao, Jiaqi Jiang, Danushka Bollegala, Min Li, and Shan Luo. Multimodal zero-shot learning for tactile texture recognition. *Robotics and Autonomous Systems*, 176:104688, 2024. 2
- [5] Enrico Donato, David Pelliccia, Matin Hosseinzadeh, Mahmood Amiri, and Egidio Falotico. Tactile object recognition

- with recurrent neural networks through a perceptive soft gripper. *IEEE Robotics and Automation Letters*, 2025. 2
- [6] Ruoxuan Feng, Jiangyu Hu, Wenke Xia, Ao Shen, Yuhao Sun, Bin Fang, Di Hu, et al. Anytouch: Learning unified static-dynamic representation across multiple visuo-tactile sensors. In *The Thirteenth International Conference on Learning Representations*, 2025. 2
- [7] Hao Fu, Fengyu Yang, Boyang Wang, Wei Ji, Hanbin Zhao, Chao Zhang, Roger Zimmermann, and Hui Qian. Visuo-tactile class-incremental learning. *ACM Transactions on Multimedia Computing, Communications and Applications*, 21(11), Nov. 2025. 2
- [8] Chenxu Guo, Qi Zhao, Shuchang Lyu, Binghao Liu, Chunlei Wang, Lijiang Chen, and Guangliang Cheng. Decision boundary optimization for few-shot class-incremental learning. In *Proceedings of the IEEE/CVF International Conference on Computer Vision*, pages 3501–3511, 2023. 2
- [9] Oliver Holland, Eckehard Steinbach, R. Venkatesha Prasad, Qian Liu, Zaher Dawy, Adnan Aijaz, Nikolaos Pappas, Kishor Chandra, Vijay S. Rao, Sharief Oteafy, Mohamad Eid, Mark Luden, Amit Bhardwaj, Xun Liu, Joachim Sachs, and José Araújo. The ieee 1918.1 “tactile internet” standards working group and its standards. *Proceedings of the IEEE*, 107(2):256–279, 2019. 2, 6
- [10] Jian Jiao, Yuru Zhang, Dangxiao Wang, Xingwei Guo, and Xiaoying Sun. Haptex: A database of fabric textures for surface tactile display. In *2019 IEEE World Haptics Conference (WHC)*, pages 331–336. IEEE, 2019. 2, 6
- [11] Junsu Kim, Yunhoe Ku, and Seungryul Baek. Can synthetic images conquer forgetting? beyond unexplored doubts in few-shot class-incremental learning. In *Proceedings of the IEEE/CVF International Conference on Computer Vision*, pages 5214–5223, 2025. 2
- [12] Alex Krizhevsky, Geoffrey Hinton, et al. Learning multiple layers of features from tiny images. 2009. 2
- [13] Chenqi Li, Boyan Gao, Gabriel Davis Jones, Timothy Denison, and Tingting Zhu. Anchorinv: Few-shot class-incremental learning of physiological signals via feature space-guided inversion. In *Proceedings of the AAAI Conference on Artificial Intelligence*, volume 39, pages 14274–14282, 2025. 1, 2
- [14] Dong Li, Aijia Zhang, Junqi Gao, and Biqing Qi. An efficient memory module for graph few-shot class-incremental learning. *Advances in Neural Information Processing Systems*, 37:130084–130108, 2024. 1
- [15] Linhao Li, Yongzhang Tan, Siyuan Yang, Hao Cheng, Yongfeng Dong, and Liang Yang. Adaptive decision boundary for few-shot class-incremental learning. In *Proceedings of the AAAI Conference on Artificial Intelligence*, volume 39, pages 18359–18367, 2025. 2, 6, 7
- [16] Yanxiong Li, Wenchang Cao, Jialong Li, Wei Xie, and Qianhua He. Few-shot class-incremental audio classification using stochastic classifier. In *Interspeech 2023*, pages 4174–4178, 2023. 2
- [17] Yanxiong Li, Wenchang Cao, Jiabin Tan, Qianqian Li, and Guoqing Chen. Few-shot class-incremental audio classification using pseudoincrementally trained embedding learner and continually updated stochastic classifier. *IEEE Transactions on Audio, Speech and Language Processing*, 2025. 1, 2, 5, 6, 7
- [18] Yunzhu Li, Jun-Yan Zhu, Russ Tedrake, and Antonio Torralba. Connecting touch and vision via cross-modal prediction. In *Proceedings of the IEEE/CVF Conference on Computer Vision and Pattern Recognition*, pages 10609–10618, 2019. 2
- [19] Zhuolin Li, Ling Weng, Yuanye Zhang, Kaile Liu, and Yang Liu. Texture recognition based on magnetostrictive tactile sensor array and convolutional neural network. *AIP Advances*, 13(10), 2023. 2
- [20] Ye Liu and Meng Yang. Sec-prompt: Semantic complementary prompting for few-shot class-incremental learning. In *Proceedings of the Computer Vision and Pattern Recognition Conference*, pages 25643–25656, 2025. 2
- [21] Tian-Fang Ma, Wei-Long Zheng, and Bao-Liang Lu. Few-shot class-incremental learning for eeg-based emotion recognition. In *International Conference on Neural Information Processing*, pages 445–455. Springer, 2022. 2
- [22] Keon-Hee Park, Kyungwoo Song, and Gyeong-Moon Park. Pre-trained vision and language transformers are few-shot incremental learners. In *Proceedings of the IEEE/CVF Conference on Computer Vision and Pattern Recognition*, pages 23881–23890, 2024. 2, 6, 7
- [23] Can Peng, Kun Zhao, Tianren Wang, Meng Li, and Brian C Lovell. Few-shot class-incremental learning from an open-set perspective. In *European Conference on Computer Vision*, pages 382–397. Springer, 2022. 2
- [24] Olga Russakovsky, Jia Deng, Hao Su, Jonathan Krause, Sanjeev Satheesh, Sean Ma, Zhiheng Huang, Andrej Karpathy, Aditya Khosla, Michael Bernstein, et al. Imagenet large scale visual recognition challenge. *International Journal of Computer Vision*, 115(3):211–252, 2015. 2
- [25] Jinxin Shi, Jiabao Zhao, Yifan Yang, Xingjiao Wu, Jiawen Li, and Liang He. Lark: Low-rank updates after knowledge localization for few-shot class-incremental learning. In *Proceedings of the IEEE/CVF International Conference on Computer Vision*, pages 3607–3617, 2025. 2
- [26] Matti Stesse, Yannik Boeck, and Eckehard Steinbach. Content-based surface material retrieval. In *2017 IEEE World Haptics Conference (WHC)*, pages 352–357. IEEE, 2017. 2, 6
- [27] Le Sun, Mingyang Zhang, Benyou Wang, and Prayag Tiwari. Few-shot class-incremental learning for medical time series classification. *IEEE Journal of Biomedical and Health Informatics*, 28(4):1872–1882, 2023. 2
- [28] Zhen Tan, Kaize Ding, Ruocheng Guo, and Huan Liu. Graph few-shot class-incremental learning. In *Proceedings of the Fifteenth ACM International Conference on Web Search and Data Mining*, pages 987–996, 2022. 2
- [29] Xiaoyu Tao, Xiaopeng Hong, Xinyuan Chang, Songlin Dong, Xing Wei, and Yihong Gong. Few-shot class-incremental learning. In *Proceedings of the IEEE/CVF Conference on Computer Vision and Pattern Recognition*, pages 12183–12192, 2020. 2
- [30] Catherine Wah, Steve Branson, Peter Welinder, Pietro Perona, and Serge Belongie. The caltech-ucsd birds-200-2011 dataset. 2011. 2
- [31] Lina Wei, Yuhang Ma, Zhongsheng Lin, Fangfang Wang, Canghong Jin, Hanbin Zhao, and Dapeng Chen. Few-shot incremental multi-modal learning via touch guidance and imaginary vision synthesis. In *Proceedings of the Thirty-Fourth International Joint Conference on Artificial Intelligence*, pages 2045–2053, 2025. 1, 2
- [32] Wufei Xie, Yalin Wang, Chenliang Liu, Zhaohui Jiang, and Xue Yang. Flexi-fscil: Adaptive knowledge retention for

breaking the stability-plasticity dilemma in few-shot class-incremental learning. In *Proceedings of the IEEE/CVF International Conference on Computer Vision*, pages 2451–2460, 2025. 2

- [33] Yating Xie, Hongyu Cheng, Chaocheng Yuan, Limin Zheng, Zhengchun Peng, and Bo Meng. Deep learning-assisted object recognition with hybrid triboelectric-capacitive tactile sensor. *Microsystems & Nanoengineering*, 10(1):165, 2024. 2
- [34] Fengyu Yang, Chenyang Ma, Jiacheng Zhang, Jing Zhu, Wenzhen Yuan, and Andrew Owens. Touch and go: learning from human-collected vision and touch. In *Proceedings of the 36th International Conference on Neural Information Processing Systems*, pages 8081–8103, 2022. 2
- [35] Rodrigo Zenha, Brice Denoun, Andrea Cavallaro, Alexandre Bernardino, and Lorenzo Jamone. Let’s dense: a novel protocol for efficiently collecting dense and diverse data for tactile slip detection in robotic grasping. *npj Robotics*, 3(1):36, 2025. 2
- [36] Chi Zhang, Nan Song, Guosheng Lin, Yun Zheng, Pan Pan, and Yinghui Xu. Few-shot incremental learning with continually evolved classifiers. In *Proceedings of the IEEE/CVF Conference on Computer Vision and Pattern Recognition*, pages 12455–12464, 2021. 2
- [37] Xi Zhao, Zhongda Sun, and Chengkuo Lee. Augmented tactile perception of robotic fingers enabled by ai-enhanced triboelectric multimodal sensors. *Advanced Functional Materials*, 34(49):2409558, 2024. 2
- [38] Da-Wei Zhou, Fu-Yun Wang, Han-Jia Ye, Liang Ma, Shiliang Pu, and De-Chuan Zhan. Forward compatible few-shot class-incremental learning. In *Proceedings of the IEEE/CVF Conference on Computer Vision and Pattern Recognition*, pages 9046–9056, 2022. 2
- [39] Yixiong Zou, Shanghang Zhang, Haichen Zhou, Yuhua Li, and Ruixuan Li. Compositional few-shot class-incremental learning. In *International Conference on Machine Learning*, pages 62964–62977. PMLR, 2024. 2, 6, 7

A Log-Mel Spectrogram Parameter Settings

Table 5 Shared log-Mel spectrogram parameters used for both Friction and LMT108 (the only difference is the sampling rate).

Parameter	Setting
FFT size	128
Window length (samples)	128
Hop length (samples)	16
Window function	Hann
Number of Mel bins	64

In our implementation, the tactile signal is converted into a log-Mel spectrogram by (i) computing the STFT magnitude spectrogram with a Hann window, (ii) projecting it onto a Mel filterbank, and (iii) applying logarithmic compression. The log-Mel extractor is shared across datasets, and thus the parameter settings are identical for both Friction and LMT108, except for the sampling rate: Friction operates at a sampling rate of 1000 Hz, while LMT108 operates at 10000 Hz. Table 5 lists the key log-Mel spectrogram parameters used in this work.

B Additional ablation on LMT108 dataset.

We also conduct ablation studies on the LMT108 dataset to assess the contributions of CaT-FSCIL. Results are summarized in table 6 and fig. 6. We make three main observations.

We observe a notable contrast between HapTex and LMT108. On LMT108, adding CaT does not consistently improve base-session accuracy, yet it improves performance in later incremental sessions. A plausible explanation is that LMT108 involves stronger and more heterogeneous acquisition-context shifts, and some context regimes are sparsely represented across classes. Under this regime, methods without explicit canonicalization may latch onto context-specific shortcuts that appear predictive on base classes but fail to transfer, causing accelerated degradation during incremental learning.

From this perspective, the benefit of CaT on LMT108 is primarily reflected in reduced context dependence rather than immediate gains on the base session. This reduction yields more stable prototypes and decision boundaries as new classes arrive under limited and shifted context coverage. UCPC further strengthens this effect by using context uncertainty to calibrate prototype shrinkage and boundary sharpness, which noticeably alleviates forgetting. In contrast, \mathcal{L}_{CaT} improves robustness mainly by enhancing context estimation and enforcing canonicalization stability. While beneficial, its gains are smaller than UCPC under highly complex context variability. Overall, the results support that each component addresses a complementary failure mode, and their coupling

Table 6 Ablation study on LMT108 dataset.

CaT	\mathcal{L}_{CaT}	UCPC	Accuracy in each session (%) \uparrow											PD \downarrow	AA \uparrow	ADR \downarrow
			0	1	2	3	4	5	6	7	8	9				
×	×	×	40.84	19.29	15.52	12.26	11.01	10.87	9.62	8.58	8.80	8.32	32.52	14.51	13.00	
✓	×	×	40.45	30.43	26.48	24.33	21.42	20.22	18.45	18.27	16.75	15.18	25.27	23.20	9.09	
✓	×	✓	40.79	36.94	31.42	28.08	25.22	23.71	21.26	20.70	19.19	17.93	22.86	26.52	7.80	
✓	✓	×	42.51	35.18	30.45	28.21	24.20	22.49	20.80	20.17	18.82	17.37	25.14	26.02	8.43	
✓	✓	✓	42.54	40.26	36.02	33.06	29.27	27.01	25.48	24.58	22.75	20.94	21.60	30.19	6.79	

leads to the best performance on LMT108.

criterion optimized during training and remains comparable across different sampling realizations and classes.

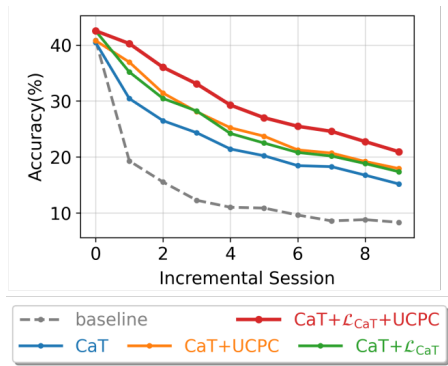


Figure 6 Ablation study on LMT108 dataset.

C Why we use the ℓ_1 norm for context consistency and uncertainty

Both the pseudo-context consistency loss in section 3.4 and the context uncertainty in section 3.5 quantify canonicalization stability by comparing two canonicalized log-Mel spectrograms. We use the ℓ_1 norm for these comparisons for two reasons.

Robustness to heavy-tailed and localized deviations. In tactile sensing, time–frequency representations often exhibit localized, high-magnitude deviations caused by transient contact dynamics (*e.g.*, micro-slip and intermittent impacts) and other unmodeled residual effects. Such deviations are typically sparse in the spectrogram domain and lead to heavy-tailed differences between two canonicalized representations. Compared to ℓ_2 , the ℓ_1 norm is less dominated by a small number of large-magnitude bins, yielding a more robust and stable learning signal when enforcing canonicalization consistency.

Alignment between the training objective and the uncertainty score. UCPC treats uncertainty as instability under pseudo-context perturbations. Using the same ℓ_1 deviation for both \mathcal{L}_{CaT} and the uncertainty computation ensures that the uncertainty score is directly aligned with the stability